

Freeze-out parameters from continuum extrapolated lattice data

Sz. Borsányi^{*1}, Z. Fodor^{1,2,3}, S. D. Katz^{2,4}, S. Krieg^{1,3}, C. Ratti⁵, K. K. Szabó¹

¹ *Department of Physics, Wuppertal University, Gausstr. 20, D-42119 Wuppertal, Germany*

² *Inst. for Theoretical Physics, Eötvös University,*

Pázmány P. sétány 1/A, H-1117 Budapest, Hungary

³ *Jülich Supercomputing Centre, Forschungszentrum Jülich, D-52425 Jülich, Germany*

⁴ *MTA-ELTE "Lendület" Lattice Gauge Theory Research Group,*

Pázmány P. sétány 1/A, H-1117 Budapest, Hungary

⁵ *Dip. di Fisica, Università di Torino and INFN, Sezione di Torino*

via Giuria 1, I-10125 Torino, Italy

E-mail: borsanyi@uni-wuppertal.de

We present continuum extrapolated lattice results for the higher order fluctuations of conserved charges in high temperature Quantum Chromodynamics. Through the matching of the grand canonical ensemble on the lattice to the net charge and net baryon distribution realized in heavy ion experiments the temperature and the chemical potential may be estimated at the time of chemical freeze-out.

31st International Symposium on Lattice Field Theory - LATTICE 2013

July 29 - August 3, 2013

Mainz, Germany

^{*}Speaker.

1. Introduction

Heavy ion experiments at the Large Hadron Collider (LHC) and the Relativistic Heavy Ion Collider (RHIC) have set out the goal to produce and study new forms of strongly interacting matter, such as the quark gluon plasma. Besides direct emissions, we can observe this matter at the point of break-up through the hadrons leaving the system. Prominent approaches include the hydrodynamical modelling of the angular distribution and the study of the event-by-event distribution of conserved charges [1].

The chemical freeze-out, defined as the last inelastic scattering of hadrons before detection, has already been studied in terms of the statistical hadronization model by fitting a chemical potential and a temperature parameter to the pion, kaon, proton and other accessible yields from experiment [2, 3]. For higher collision energies smaller chemical potential are realized at freeze-out. Repeating the analysis for a series of beam energies provide a manifold of $(T - \mu)$ pairs on the phase diagram, the freeze-out curve in Fig. 1.

While we know from lattice simulations that the QCD transition is a crossover at zero chemical potential [4], a critical end point and a first order transition line may exist in the $(T - \mu)$ plane. Its experimental search is based on the analysis of event-by-event fluctuations [5].

Parallel to the experimental effort lattice field theory has been able to describe the QCD transition in an increasing detail. The transition temperature has been determined [6, 7], and the curvature of the transition line was also given [8]. The equation of state has been calculated at zero [9, 10] and small chemical potentials [11]. Quark number susceptibilities have also been determined both for strange as well as light flavors [12, 13]. All these results have been subject to a continuum extrapolation.

The ever-increasing accuracy of fluctuation measurements at RHIC and LHC allows us today to make direct comparisons of lattice results with data. The STAR experiment has recently published the beam-energy and centrality dependence of the net-proton distribution [14]. For the net electric charge distribution there are preliminary results available both from the STAR [15, 16] and from the PHENIX collaboration [17].

The strategy for a successful comparison between theory and experiment has been long worked on [18, 19, 20]. Here we use the observables suggested in Ref. [21]. The fluctuations for a conserved quantum number, such as electric charge, are measured in a sub-system, small enough to behave like a grand canonical ensemble, yet large enough to behave like an ensemble. The selection of a subsystem is accomplished through cuts in rapidity and transverse momentum. Still, the fluctuations or even the mean value of net charge depends on the unknown subvolume. To cancel this factor ratios are considered, such as mean/variance, which was described as a baryometer in Refs. [20, 21]. Other relevant combinations are listed in Eq. (2.2).

At zero chemical potential the mean and skewness vanish, leaving us only with the kurtosis and variance to work with at the energies of LHC. RHIC, however, works at non-zero chemical potentials. There we expand the lattice results around zero chemical potential and extrapolate to small but finite values and use then the mean and the skewness, which are now non-zero. In Ref. [21] these observables were used as baryometer and thermometer, respectively.

The rules for such an extrapolation are given by the experimental setting: there is no strangeness input in the colliding nuclei, and the ratio of protons and neutrons in the gold or lead atoms prede-

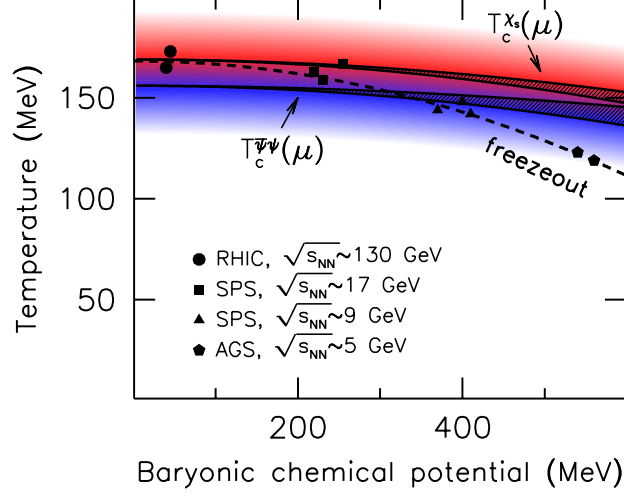


Figure 1: The QCD phase diagram for small chemical potentials [8]. A temperature and a chemical potential has been fitted in terms of the statistical hadronization model for every collision energy [2, 3]. For comparison we show the crossover lines based on two observables from lattice simulations [8].

termine the charge-to-baryon ratio in the outgoing hadrons as well. Thus:

$$\langle S \rangle = 0, \quad \langle Q \rangle = 0.4 \langle B \rangle. \quad (1.1)$$

These conditions can be respected if we introduce a strange and electric charge chemical potential in addition to the baryochemical potential, as it has already been a method in the statistical hadronization model.

2. Fluctuations from the lattice

We generated finite temperature ensembles using the three-level Symanzik improved gauge action with dynamical stout-improved staggered fermions (see Ref. [22]). The temporal extent of the lattices determine the lattice spacing at a given temperature, we use $N_t = 6, 8, 10, 12, 16$ (around T_c these translate to the lattice spacings of $a = 0.22, 0.16, 0.13, 0.11$ and 0.08 fm, respectively). At every lattice spacing and temperature we stored and analyzed every 10th configuration in the rational hybrid Monte Carlo streams.

In a grand canonical ensemble we obtain the fluctuations as derivatives of the partition function with respect to the chemical potentials:

$$\frac{\chi_{lmn}^{BSQ}}{T^{l+m+n}} = \frac{\partial^{l+m+n}(p/T^4)}{\partial(\mu_B/T)^l \partial(\mu_S/T)^m \partial(\mu_Q/T)^n}. \quad (2.1)$$

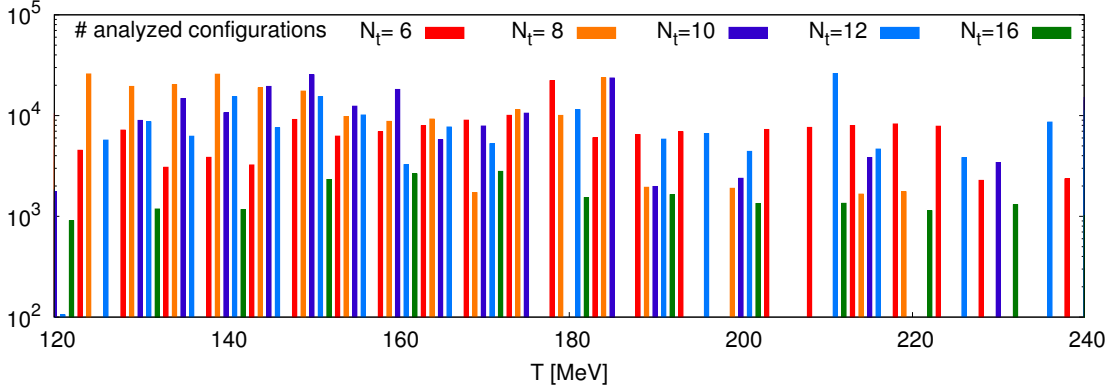


Figure 2: Statistics behind the fluctuation calculations. The stored configurations have been separated by 10 HMC trajectories, each. Each configuration was analyzed by $(128 \dots 256) \times 4$ random sources.

and they are related to the moments of the distributions of the corresponding conserved charges by

$$\begin{aligned} \text{mean} : M &= \chi_1 & \text{variance} : \sigma^2 &= \chi_2 \\ \text{skewness} : S &= \chi_3 / \chi_2^{3/2} & \text{kurtosis} : \kappa &= \chi_4 / \chi_2^2. \end{aligned} \quad (2.2)$$

With these moments we can express the volume independent ratios

$$\begin{aligned} S\sigma &= \chi_3 / \chi_2 & ; & \quad \kappa\sigma^2 = \chi_4 / \chi_2 \\ M / \sigma^2 &= \chi_1 / \chi_2 & ; & \quad S\sigma^3 / M = \chi_3 / \chi_1. \end{aligned} \quad (2.3)$$

The chemical potential dependence enters through the fermion determinant ($\det M_i$), allowing for one μ_i parameter for each of the three dynamical flavor $i = u, d, s$. The actual observables are based on the derivatives of the logarithm of these determinants:

$$A_j = \frac{d}{d\mu_j} \log(\det M_j)^{1/4} = \frac{1}{4} \text{Tr} M_j^{-1} M_j', \quad (2.4)$$

$$B_j = \frac{d^2}{(d\mu_j)^2} \log(\det M_j)^{1/4} = \frac{1}{4} \text{Tr} \left(M_j'' M_j^{-1} - M_j' M_j^{-1} M_j' M_j^{-1} \right), \quad (2.5)$$

$$\begin{aligned} C_j = \frac{d^3}{(d\mu_j)^3} \log(\det M_j)^{1/4} &= \frac{1}{4} \text{Tr} \left(M_j' M_j^{-1} - 3M_j'' M_j^{-1} M_j' M_j^{-1} \right. \\ &\quad \left. + 2M_j' M_j^{-1} M_j' M_j^{-1} M_j' M_j^{-1} \right), \end{aligned} \quad (2.6)$$

$$\begin{aligned} D_j = \frac{d^4}{(d\mu_j)^4} \log(\det M_j)^{1/4} &= \frac{1}{4} \text{Tr} \left(M_j'' M_j^{-1} - 4M_j' M_j^{-1} M_j' M_j^{-1} + 12M_j'' M_j^{-1} M_j' M_j^{-1} M_j' M_j^{-1} \right. \\ &\quad \left. - 3M_j'' M_j^{-1} M_j'' M_j^{-1} - 6M_j' M_j^{-1} M_j' M_j^{-1} M_j' M_j^{-1} M_j' M_j^{-1} \right). \end{aligned} \quad (2.7)$$

We calculate these traces for every configuration using $(128 \dots 256) \times 4$ random sources. The final derivatives emerge as connected and disconnected contributions, e.g. to second order we have

$$\partial_i \partial_j \log Z = \langle A_i A_j \rangle + \delta_{ij} \langle B_i \rangle. \quad (2.8)$$

Where products of diagrams appear, a disjoint set of random sources are used, like here in A_i and A_j , even when $i = j$. The first (disconnected) term is responsible for most of the noise, lattice artefacts, on the other hand, come mainly from the connected contributions.

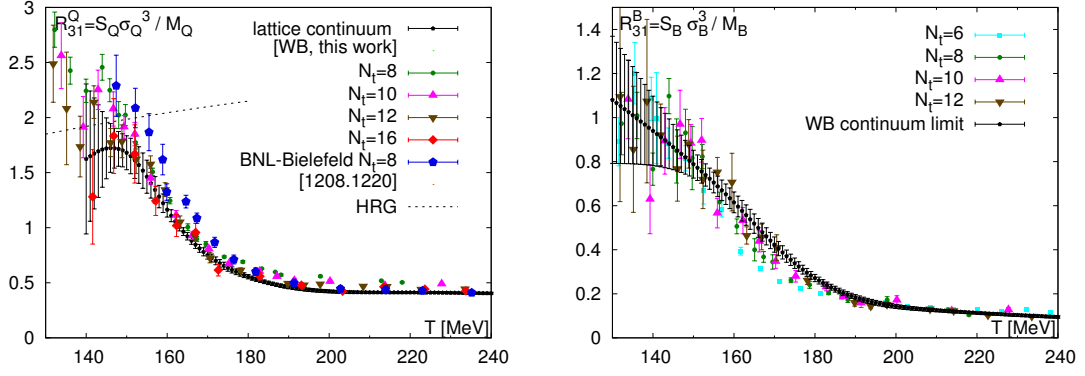


Figure 3: Lattice results on the skewness ratio for the charge (left) and the baryon number (right). The colored symbols correspond to lattice QCD simulations at finite- N_t . Black points correspond to the continuum extrapolation [23]; blue pentagons are the $N_t = 8$ results from the BNL-Bielefeld collaboration [21]

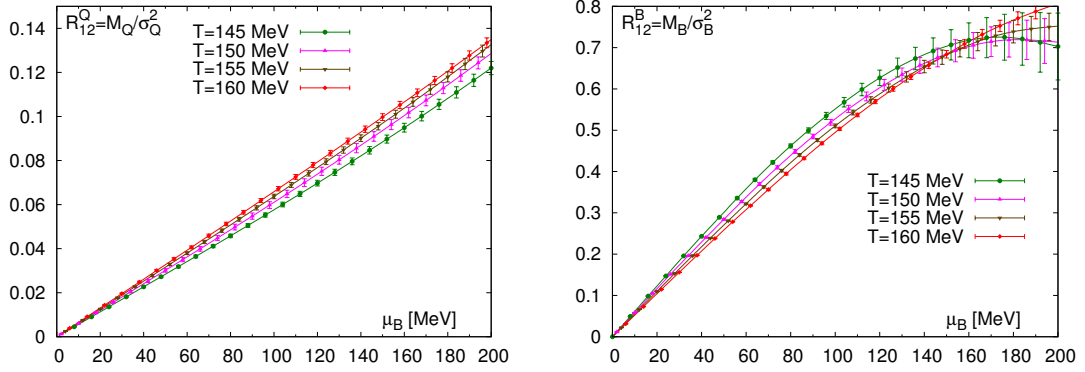


Figure 4: R_{12}^Q as a function of μ_B : the different colors correspond to the continuum extrapolated lattice QCD results, calculated in a range of temperatures around the QCD crossover [23].

3. Results

The quantities that we look at, in order to extract the freeze-out temperature and baryon chemical potential, are the ratios $R_{31}^Q(T, \mu_B) = \chi_3^Q / \chi_1^Q$ and $R_{12}^Q(T, \mu_B) = \chi_1^Q / \chi_2^Q$ for small chemical potentials, where $\mu_Q(\mu_B)$ and $\mu_S(\mu_B)$ are chosen to satisfy Eqs. (1.1). We also calculated the analogous baryon fluctuations. For details, see the journal version of this work [23].

In Fig. 3 we show the ratios R_{31}^Q (left) and R_{31}^B (right) as a function of the temperature. The continuum extrapolations are shown as black dots. For the charge fluctuations we used five lattice spacings. Baryon fluctuations are plagued by greater noise, but are less sensitive to cut-off effects, here we used four spacings. Charge fluctuation results from the BNL-Bielefeld collaboration corresponding to $N_t = 8$ (from Ref. [21]) are also shown for comparison.

In Fig. 4 we show our results for R_{12}^Q as a function of the baryon chemical potential: the different curves correspond to different temperatures, in the range where freeze-out is expected. Such expectations may come from the arguments in Ref. [24] supporting a freeze-out just below the tran-

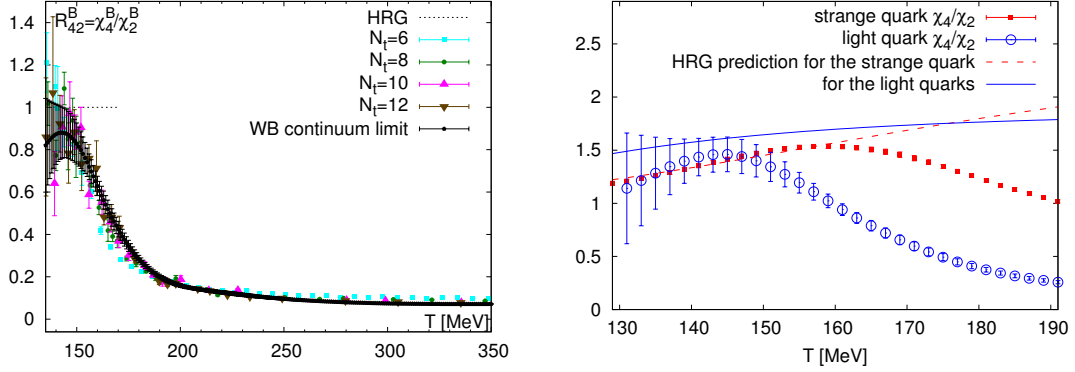


Figure 5: The baryon number (left) and flavor specific (right) kurtosis ($\kappa \times \sigma^2$) prediction from lattice QCD. These parameters are in principle accessible to LHC experiments, and may be used to define the freeze-out temperature for specific flavors, or to the system as a whole.

sition. Alternative hints come from the existing estimates from the statistical hadronization model [2, 3]. Similarly to the electric charge fluctuations, R_{31}^B will allow us to constrain the temperature and using R_{12}^B we can then obtain μ_B .

Notice that the ordering of the temperatures in Fig. 4 (left) and (right) is opposite. Thus, whether the chemical potentials from the charge and the baryon (proton) fluctuations deliver consistent results will very much depend on the associated temperature, which we can extract from the skewness analysis. A possible source for inconsistencies might be the comparison of proton fluctuation data with baryon fluctuations from the lattice, and also the remnant effects of baryon number conservation [25]. A cross-check between the freeze-out parameters from proton and electric charge data also test the basic assumption of equilibrium at the time of freeze-out.

Finally we show the kurtosis data in the continuum limit in Fig. 5. The kurtosis of baryon number and light vs. strange quark numbers show different sensitivity to temperature, so are the maxima and the deviation point from the hadron resonance gas prediction flavor dependent. The great question that the experiment will have to decide is whether the freeze-out temperatures themselves are flavor dependent [26].

Acknowledgments: This project was funded by the DFG grant SFB/TR55. The work of C. Ratti is supported by funds provided by the Italian Ministry of Education, Universities and Research under the Fibr Research Grant RBFR0814TT. S. D. Katz is funded by the ERC grant ((FP7/2007-2013)/ERC No 208740) as well as the "Lendület" program of the Hungarian Academy of Sciences ((LP2012-44/2012). The numerical simulations were in part performed the GPU cluster at the Wuppertal University as well as on QPACE, funded by the DFG. We acknowledge PRACE for awarding us access to the Blue Gene/Q system (JUQUEEN) at Forschungszentrum Jülich, Germany.

References

- [1] B. Hippolyte and D. H. Rischke, Nucl. Phys. A **904-905** (2013) 318c [arXiv:1211.6714 [nucl-ex]].
- [2] A. Andronic, P. Braun-Munzinger and J. Stachel, Nucl. Phys. A **772** (2006) 167 [nucl-th/0511071] ; Phys. Lett. B **673** (2009) 142 [Erratum-ibid. B **678** (2009) 516] [arXiv:0812.1186 [nucl-th]].

- [3] J. Cleymans, H. Oeschler, K. Redlich and S. Wheaton, *Phys. Rev. C* **73** (2006) 034905 [hep-ph/0511094].
- [4] Y. Aoki, G. Endrodi, Z. Fodor, S. D. Katz and K. K. Szabo, *Nature* **443**, 675 (2006)
- [5] M. A. Stephanov, K. Rajagopal and E. V. Shuryak, *Phys. Rev. D* **60**, 114028 (1999) [hep-ph/9903292].
- [6] Y. Aoki, *et al.* *Phys. Lett. B* **643** (2006) 46; Y. Aoki, *et al.* *JHEP* **0906** (2009) 088; S. Borsanyi *et al.* [Wuppertal-Budapest Coll.], *JHEP* **1009**, 073 (2010)
- [7] A. Bazavov, T. Bhattacharya, M. Cheng, C. DeTar, H. T. Ding, S. Gottlieb, R. Gupta and P. Hegde *et al.*, *Phys. Rev. D* **85** (2012) 054503 [arXiv:1111.1710 [hep-lat]].
- [8] G. Endrodi, Z. Fodor, S. D. Katz and K. K. Szabo, *JHEP* **1104** (2011) 001 [arXiv:1102.1356 [hep-lat]].
- [9] S. Borsanyi, G. Endrodi, Z. Fodor, A. Jakovac, S. D. Katz, S. Krieg, C. Ratti and K. K. Szabo, *JHEP* **1011** (2010) 077 [arXiv:1007.2580 [hep-lat]].
- [10] S. Borsanyi, Z. Fodor, C. Hoelbling, S. D. Katz, S. Krieg and K. K. Szabo, arXiv:1309.5258 [hep-lat].
- [11] S. Borsanyi, G. Endrodi, Z. Fodor, S. D. Katz, S. Krieg, C. Ratti and K. K. Szabo, *JHEP* **1208** (2012) 053 [arXiv:1204.6710 [hep-lat]].
- [12] S. Borsanyi, Z. Fodor, S. D. Katz, S. Krieg, C. Ratti and K. Szabo, *JHEP* **1201** (2012) 138 [arXiv:1112.4416 [hep-lat]].
- [13] A. Bazavov *et al.* [HotQCD Collaboration], *Phys. Rev. D* **86** (2012) 034509 [arXiv:1203.0784 [hep-lat]].
- [14] L. Adamczyk *et al.* [STAR Collaboration], arXiv:1309.5681 [nucl-ex].
- [15] D. McDonald [STAR Coll.], arXiv:1210.7023 [nucl-ex].
- [16] N. R. Sahoo [STAR Coll.], arXiv:1212.3892 [nucl-ex].
- [17] J. T. Mitchell [PHENIX Collaboration], *Nucl. Phys. A* **904-905** (2013) 903c [arXiv:1211.6139 [nucl-ex]].
- [18] S. Jeon and V. Koch, *Phys. Rev. Lett.* **85**, 2076 (2000)
- [19] M. Asakawa, U. W. Heinz and B. Muller, *Phys. Rev. Lett.* **85**, 2072 (2000)
- [20] F. Karsch, *Central Eur. J. Phys.* **10** (2012) 1234 [arXiv:1202.4173 [hep-lat]].
- [21] A. Bazavov, H. T. Ding, P. Hegde, O. Kaczmarek, F. Karsch, E. Laermann, S. Mukherjee and P. Petreczky *et al.*, *Phys. Rev. Lett.* **109** (2012) 192302 [arXiv:1208.1220 [hep-lat]].
- [22] Y. Aoki, *et al.* *JHEP* **0601**, 089 (2006)
- [23] S. Borsanyi, Z. Fodor, S. D. Katz, S. Krieg, C. Ratti and K. K. Szabo, *Phys. Rev. Lett.* **111** (2013) 062005 [arXiv:1305.5161 [hep-lat]].
- [24] P. Braun-Munzinger, J. Stachel and C. Wetterich, *Phys. Lett. B* **596** (2004) 61
- [25] A. Bzdak, V. Koch and V. Skokov, *Phys. Rev. C* **87** (2013) 014901 [arXiv:1203.4529 [hep-ph]].
- [26] R. Bellwied, S. Borsanyi, Z. Fodor, S. DKatz and C. Ratti, *Phys. Rev. Lett.* **111** (2013) 202302 [arXiv:1305.6297 [hep-lat]].